Journal of the Optical Society of America A
OPTICS, IMAGE SCIENCE, AND VISION

Compressive sensing approaches for the prediction of scattered electromagnetic fields

CHANDAN BHAT,† KARTEEKEYA SASTRY,† AND UDAY K. KHANKHOJE*

Department of Electrical Engineering, Indian Institute of Technology, Madras, Chennai, India
**Corresponding author: uday@ee.iitm.ac.in*

Received 15 January 2020; revised 21 May 2020; accepted 29 May 2020; posted 1 June 2020 (Doc. ID 388136); published 25 June 2020

We present a novel method based on Huygens' principle and compressive sensing to predict the electromagnetic (EM) fields in arbitrary scattering environments by making a few measurements of the field. In doing so, we assume a homogeneous medium between the scatterers, though we do not assume prior knowledge of the permittivities or the exact geometry of the scatterers. The major contribution of this work is a compressive sensing-based subspace optimization method (CS-SOM). Using this, we show that the EM fields in an indoor situation with up to four scattering objects can be reconstructed with approximately 12% error, when the number of measurements is only 55% of the number of variables used to formulate the problem. Our technique departs significantly from traditional ray tracing approaches. We use a surface integral formulation which captures wave-matter interactions exactly, leverage compressive sensing techniques so that field measurements at a few random locations suffice, and apply Huygens' principle to predict the fields at any location in space.

https://doi.org/10.1364/JOSAA.388136

1. INTRODUCTION

Reconstruction of electromagnetic (EM) fields in a scattering environment is a fundamental problem, with many practical applications such as radar cross-section estimation [1], indoor positioning [2,3], Wi-Fi access point planning [4], and such others. Traditional approaches to this problem use ray tracing methods [5–7]. These techniques are valid only in the high-frequency regime, suffer from large errors in near-field estimation, and face difficulties in modeling multiple scattering events (Fig. 3 in [8]). These drawbacks may limit their applicability significantly. In this paper, we overcome these limitations by proposing new techniques that model wave-matter interactions exactly using surface integral formulations. This characterization enables accurate prediction of EM fields in *arbitrary* scattering environments.

A. Problem Statement

The general real world problem that we aim to address is as follows: consider a room with some objects such as tables and chairs in which an active antenna (e.g., a Wi-Fi router) is placed. Can the electromagnetic field at every point inside the room be predicted?

It is desirable to solve this problem by making the least possible number of field measurements. For this reason, interpolation-based techniques are impractical because field variations on a sub-wavelength scale dictate a high density of measurements. Motivated by this, we present techniques that can reconstruct fields by making few measurements. A major strength of our approach is that we do not need to know the permittivity of the objects; only a rough estimate of their locations is sufficient. That said, we assume that the medium between the scatterers is homogeneous. An abstraction of the real world problem stated above is shown schematically in Fig. 1 by means of a two-dimensional (2D) scattering problem.

B. Our Approach

According to Huygens' principle, the scattered field at a point can be expressed as a convolution between the free space Green's function and the tangential electric and magnetic fields on the surface of the scatterers. Additionally, the Extinction theorem enforces certain relations between the tangential electric and magnetic fields [9]. Thus, estimating these tangential fields by using the above relations points the way to predicting the scattered fields outside the scattering objects. Further, it is empirically observed that these tangential fields are sparse in certain bases (we substantiate this later in the text). By leveraging this prior information and using the theory of compressive sensing, we can bring down the number of measurements required.

In the discrete world, the relation between the measurements, $\boldsymbol{b} \in \mathbb{C}^M$, and the tangential fields, $\boldsymbol{x} \in \mathbb{C}^N$, is given by the system matrix, A, as $\boldsymbol{b} = A\boldsymbol{x} + \boldsymbol{v}$, where $\boldsymbol{v}$ represents measurement noise, M is the number of measurements, and N the number of variables used to describe the tangential fields. Additionally,

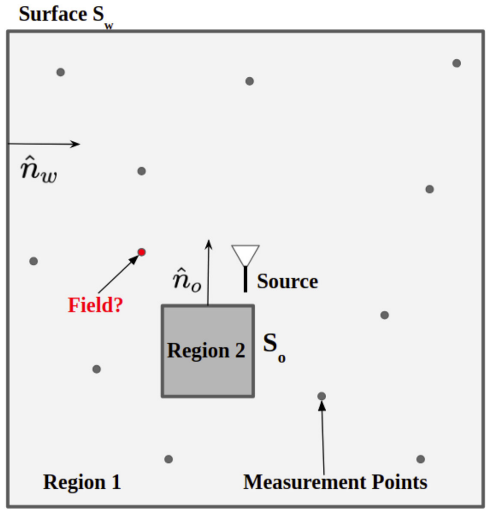

Fig. 1. Schematic of the problem statement: can the field be predicted anywhere in Region 1 (a homogeneous medium) by making a few measurements in the presence of an obstacle denoted by Region 2? S_w is the inner surface of the enclosing wall and S_o is the outer surface of the scatterer. $\hat{n}_w$ and $\hat{n}_o$ are normals to the scattering surfaces of the wall and object, respectively.

the Extinction theorem gives the following relation between the tangential fields: $A_s\boldsymbol{x} = \boldsymbol{b}_s$, where $\boldsymbol{b}_s \in \mathbb{C}^{N/2}$ contains the incident field, and A_s is termed as the state matrix. The field predicted, $\boldsymbol{f} \in \mathbb{C}^S$, is expressed in terms of the prediction matrix B, as $\boldsymbol{f} = B\boldsymbol{x}$, where S is the number of locations where the field is desired. Therefore, the problem boils down to estimating $\boldsymbol{x}$ given $\{\boldsymbol{b}, \boldsymbol{b}_s\}$ which is a convex optimization problem with known solution strategies [10,11].

The problem of recovering a higher dimensional signal from lower dimensional field measurements has been widely studied in the inverse imaging community [12–14]. In particular, a family of so-called subspace optimization methods (SOMs) [15] provide a convenient framework to split the desired signal into two orthogonal subspaces and to independently recover each component. In recent work [16], we have shown an efficient scheme to recover one component from the field data and the other based on a priori information.

C. Our Contributions

To the best of our knowledge, this approach of using the surface integral formulation along with compressive sensing for solving the problem of field prediction has not been reported earlier. We propose a compressive sensing-based subspace optimization method (CS-SOM), that works by splitting a signal into two orthogonal vector subspaces and uses signal sparsity in suitable domains to achieve high accuracy field predictions. Using this technique, we show that in a scattering environment (such as in the schematic of Fig. 1), the EM field (in Region 1) can be reconstructed with approximately 12% error and the tangential fields on scatterer surfaces can be reconstructed with approximately 22% error, when the number of measurements is only 55% of the number of variables used to formulate the problem.

D. Paper Organization

The rest of the paper is organized as follows: we formally define the problem statement in Section 2. Then, Section 3 explains the theoretical details of the CS-SOM algorithm used to solve the stated problem. Numerical results for the field prediction are presented in Section 4. We conclude with a discussion of open issues, limitations, and possible applications of our techniques in Section 5.

2. PROBLEM FORMULATION

A. Governing Physics

The EM field at any location can be obtained using Huygens' principle, which states that the field at any location is the superposition of primary (incident fields) and secondary sources located on scatterer surface(s) (scattered fields) [9]. The schematic shown in Fig. 1 shows a 2D computational domain which is illuminated by a transverse magnetic (TM) polarization field. The z-component of the electric field in Region 1, $\phi(\vec{r})$, can be expressed using Huygens' principle [17] as follows:

$$\begin{aligned}\phi(\vec{r}) &= \phi_{\text{in}}(\vec{r}) \\ &- \oint_{S_w} [g(\vec{r},\vec{r}')\nabla'\phi_w(\vec{r}') - \phi_w(\vec{r}')\nabla' g(\vec{r},\vec{r}')] \cdot \hat{n}_w \mathrm{d}l' \\ &- \oint_{S_o} [g(\vec{r},\vec{r}')\nabla'\phi_o(\vec{r}') - \phi_o(\vec{r}')\nabla' g(\vec{r},\vec{r}')] \cdot \hat{n}_o \mathrm{d}l',\end{aligned} \tag{1}$$

where $g(\vec{r},\vec{r}') = -(j/4)H_0^{(2)}(k_0|\vec{r}-\vec{r}'|)$ is the free space Green's function in Region 1, $\phi_{\text{in}}(\vec{r})$ is the incident EM field due to a source, ϕ_o, ϕ_w are the tangential electric fields on the object and wall surfaces, and $\hat{n}_w$ $\hat{n}_o$ are normals to the scattering surfaces of the wall and object, respectively, as shown in Fig. 1. It can be shown that $\nabla\phi_o \cdot \hat{n}_o$ and $\nabla\phi_w \cdot \hat{n}_w$ are proportional to the tangential magnetic fields on the object and wall, respectively. S_w is the inner surface of the enclosing wall, and S_o is the surface of the scatterer; since the problem is 2D, the surface integrals are equivalent to contour integrals.

As per the Uniqueness Theorem of electromagnetics [9], it is superfluous to use *both* the tangential electric and magnetic fields over the entire surfaces to determine the field when using Huygens' principle. Indeed, the tangential electric and magnetic fields on the surface are related to themselves via the Extinction theorem. When we apply this theorem to Region 1, the following relation is obtained between the tangential field variables, $\{\phi_t(\vec{r}), \nabla\phi_t(\vec{r}) \cdot \hat{n}_t\}, t \in \{o, w\}$:

$$\begin{aligned}&- \oint_{S_w} [g(\vec{r},\vec{r}')\nabla'\phi_w(\vec{r}') - \phi_w(\vec{r}')\nabla' g(\vec{r},\vec{r}')] \cdot \hat{n}_w \mathrm{d}l' \\ &- \oint_{S_o} [g(\vec{r},\vec{r}')\nabla'\phi_o(\vec{r}') - \phi_o(\vec{r}')\nabla' g(\vec{r},\vec{r}')] \cdot \hat{n}_o \mathrm{d}l' \\ &= -\phi_{\text{in}}(\vec{r}), \quad \vec{r} \in \{S_w, S_o\}.\end{aligned} \tag{2}$$

B. Discretized Equations

We express the unknowns $\phi_w, \phi_o, (\nabla\phi_w \cdot \hat{n}_w)$ and $(\nabla\phi_o \cdot \hat{n}_o)$ in a known basis $p_n(r)$, as follows:

$$\phi_o(r) = \sum_{i=1}^{N_o} a_n^o p_n(r), \qquad \nabla\phi_o(r)\cdot\hat{n}_o = \sum_{i=1}^{N_o} b_n^o p_n(r), \tag{3}$$

$$\phi_w(r) = \sum_{i=1}^{N_w} a_n^w q_n(r), \qquad \nabla\phi_w(r)\cdot\hat{n}_w = \sum_{i=1}^{N_w} b_n^w q_n(r), \tag{4}$$

where lowercase r is reserved to denote the parametrized distance along each respective surface (S_o or S_w); $p_i(r)$, $i = 1, 2, \ldots, N_o$, and $q_i(r)$, $i = 1, 2, \ldots, N_w$ are the sets of basis functions and a_n^o, b_n^o, a_n^w and b_n^w, are the unknown coefficients. Substituting Eqs. (3) and (4) in Eq. (1), and considering M locations of field measurement, we get a linear system of equations of the following form:

$$\underbrace{\begin{bmatrix} E & F & G & H \end{bmatrix}}_{A} \underbrace{\begin{bmatrix} \boldsymbol{a}^o \\ \boldsymbol{b}^o \\ \boldsymbol{a}^w \\ \boldsymbol{b}^w \end{bmatrix}}_{\boldsymbol{x}} = \underbrace{\begin{bmatrix} \phi_s(\vec{r}_1) \\ \phi_s(\vec{r}_2) \\ \vdots \\ \phi_s(\vec{r}_M) \end{bmatrix}}_{\boldsymbol{b}} + \boldsymbol{\nu}, \tag{5}$$

where $\{E, F\} \in \mathbb{C}^{M\times N_o}$, $\{G, H\} \in \mathbb{C}^{M\times N_w}$ compose the system matrix $A \in \mathbb{C}^{M\times N}$, $x \in \mathbb{C}^N$ is a vector with vertically stacked elements $\{\boldsymbol{a}^o, \boldsymbol{b}^o\} \in \mathbb{C}^{N_o}$ and $\{\boldsymbol{a}^w, \boldsymbol{b}^w\} \in \mathbb{C}^{N_w}$, with $N = 2(N_w + N_o)$ determining the total number of unknowns. The scattered field at a location $\vec{r}_i$ is $\phi_s(\vec{r}_i)$, which is corrupted by noise given in ν.

Similarly, substituting Eqs. (3) and (4) in Eq. (2), gives the following form of the discretized "state" equation:

$$A_s \boldsymbol{x} = \underbrace{-\left[\phi_{\text{in}}(\vec{r}_1^{(s)}) \cdots \phi_{\text{in}}(\vec{r}_{\frac{N}{2}}^{(s)})\right]^T}_{\boldsymbol{b}_s}, \tag{6}$$

where $A_s \in \mathbb{C}^{\frac{N}{2}\times N}$ is the state matrix, and $\vec{r}_i^{(s)}$, $i \in [1, \frac{N}{2}]$ in this case refer to unique points along the surfaces S_o, S_w; these points are made precise once the choice of basis functions is made concrete.

One of the standard methods of *exactly* solving this linear system for the coefficients $\phi_w, \phi_o, (\nabla\phi_w \cdot \hat{n}_w)$, and $(\nabla\phi_o \cdot \hat{n}_o)$ is to combine the above equation with the Extinction theorem for the other regions (however, this requires knowledge of the scatterer permittivity) and then solve numerically by using the method of moments (MOM) [9].

C. Key Idea

Our approach is to trade off the exactness of the solution with the knowledge of the scatterer permittivity, thereby only using Eqs. (5) and (6) to *estimate* the unknown coefficients. Recall that this only involves the Green's function for Region 1 (i.e., free space), whereas the exact solution requires the Green's function for both Regions. Typically, Region 1 will always be free space, whereas Region 2 will include objects with heterogeneous permittivity, usually unknown in practical situations.

The previously mentioned estimation can be accomplished by measuring the field at a few random locations such that the right hand side vector $\boldsymbol{b}$ in Eq. (5) is known. Since the system matrix A has been constructed beforehand, the coefficients $\boldsymbol{x}$ can be estimated, and as a result, the tangential fields are known via Eqs. (3) and (4). Then, substituting these fields back in Eq. (1), we can predict the field at any point in Region 1.

Ideally we are interested in making this prediction by measuring the field at as few locations as required. This typically leads to the case of having the number of measurements, M, be less than the number of unknowns, N, i.e., A is under-determined. For this setup, the problem is formulated as follows:

1. Estimate the tangential fields by solving the following convex optimization problem:

$$\underset{\boldsymbol{x}}{\text{minimize}} \; \|A\boldsymbol{x} - \boldsymbol{b}\|_2 \le \epsilon, \; \|A_s\boldsymbol{x} - \boldsymbol{b}_s\|_2 \le \eta, \tag{7}$$

   where A, A_s, $\boldsymbol{x}$, $\boldsymbol{b}_s$ are as before, $\boldsymbol{b} \in \mathbb{C}^M$ is the vector containing noisy measurements, ϵ is an estimate of the square root of the noise variance, and η is an estimate of the discretization error in the state equation.
2. Substitute $\boldsymbol{x}$ from the previously mentioned equation into Eq. (1) and calculate the field at S locations. Let the true field at these S locations obtained from the forward solver be $\boldsymbol{f} \in \mathbb{C}^S$ (i.e., this data is generated synthetically). Then we compute the error, $e \in \mathbb{R}$ as

$$e = \|B\boldsymbol{x} - \boldsymbol{f}\|_2, \tag{8}$$

   where $B \in \mathbb{C}^{S\times N}$ is the matrix obtained from Huygens' principle Eq. (1), which when multiplied with the tangential fields $\boldsymbol{x}$ gives the estimates of the EM fields.

It is crucial to note that B is identical to A in structure; the difference arises purely due to the choice of the location $\vec{r}$ in the Green's function, $g(\vec{r}, \vec{r}')$; in A, this $\vec{r}$ corresponds to measurement locations, whereas in B, it corresponds to the locations where the field is desired. Therefore, in order to construct B, we follow the same procedure described in this section [discretize Eq. (1) by expanding the unknowns in a suitable basis and plug in those values of $\vec{r}$ where the field prediction is desired]. It is to be noted that we are interested in predicting the fields outside the object (i.e., in Region 1). To get the fields inside the objects, we need to consider the Extinction theorem, which involves knowing the exact permittivities of the objects. Also note that even though in this paper we only deal with the scalar 2D case, extensions to the 3D case or to the vector formulation are not fundamentally different.

3. COMPRESSIVE SENSING-BASED SUBSPACE OPTIMIZATION

In this section, we explain the algorithm used to solve the problem formulated in the previous section.

A. System & State Matrix

The system matrix depends on a particular choice of the basis functions, $p_i(r)$, previously introduced. To represent the tangential fields on scatterer surfaces, we use pulse basis functions defined as follows: an arbitrarily shaped contour S of length L is divided into n segments of equal length, and with r denoting the parameterized distance along the contour (the starting point on the contour is chosen arbitrarily), the ith basis function is

$$p_i(r) = \begin{cases} 1 & r_{S,i-1} \le r \le r_{S,i} \\ 0 & \text{else} \end{cases} \qquad i \in [1, n],\ 0 \le r \le L,$$

where $r_{S,i}$ denotes the parameterized distance giving the end of the i^{th} segment on S. In our case, the contour could be either the object S_o (with $n = N_o$, basis functions denoted by p), or the wall S_w (with $n = N_w$, basis functions denoted by q). In this pulse basis, the system matrix is denoted as $A_p = [E_p\ F_p\ G_p\ H_p]$, with the elements of each sub-matrix given by the corresponding lowercase symbols [18]:

$$\begin{aligned} e_{m,k} &= \int_{r_{w,k-1}}^{r_{w,k}} \frac{jk_0}{4\rho_{r_m}} H_1^{(2)}(k_0\rho_m)(\Delta\vec{R}_m \cdot \hat{n})\mathrm{d}r \\ f_{m,k} &= -\int_{r_{w,k-1}}^{r_{w,k}} \frac{j}{4} H_0^{(2)}(k_0\rho_m)\mathrm{d}r \\ g_{m,k} &= \int_{r_{o,k-1}}^{r_{o,k}} \frac{jk_0}{4\rho_{r_m}} H_1^{(2)}(k_0\rho_m)(\Delta\vec{R}_m \cdot \hat{n})\mathrm{d}r \\ h_{m,k} &= -\int_{r_{o,k-1}}^{r_{o,k}} \frac{j}{4} H_0^{(2)}(k_0\rho_m)\mathrm{d}r \end{aligned}, \tag{9}$$

where $\Delta\vec{R}_m = \vec{R}_m - \vec{R}(r)$, $\rho_m = |\Delta\vec{R}_m|$ with $\vec{R}_m$ denoting the position vector of the m^{th} measurement point, and $\vec{R}(r)$ denoting the position vector of the point on the respective contour with parameterized distance r. Similar expressions can be obtained for the elements of the state matrix by setting $\{\vec{r}_1^{(s)}, \ldots, \vec{r}_{\frac{N}{2}}^{(s)}\}$ in Eq. (6) to the midpoints of the discretized segments of the surfaces S_o and S_w (these segments are $\frac{N}{2}$ in number). Sufficient care has to be taken while evaluating the associated singular integrals.

B. Subspace Optimization Method

In order to solve this problem, we improvise on the SOM [15], typically used in the context of inverse scattering problems.

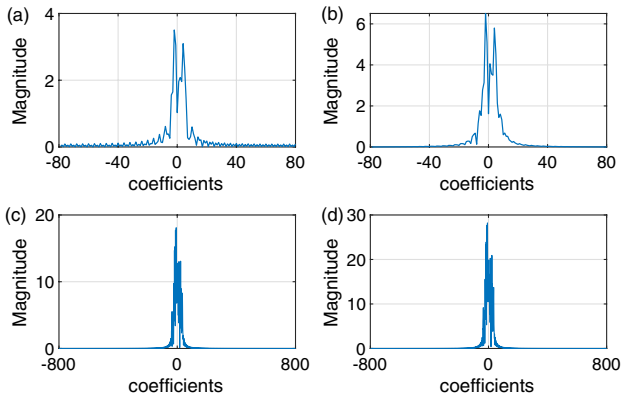

Fig. 2. DFT coefficients of the tangential fields (a) $\nabla\phi_o \cdot \hat{n}_o$, (b) ϕ_o on the scattering surface S_o, and (c) $\nabla\phi_w \cdot \hat{n}_w$, (d) ϕ_w on the scattering surface S_w as shown in Fig. 1. Most coefficients have very low magnitudes.

Here, the signal of interest is recovered from its projection in two orthogonal subspaces. Our approach begins with the singular value decomposition (SVD) of the system matrix as $A_p = \sum_i \boldsymbol{u}_i \sigma_i \boldsymbol{v}_i^H$, where $\boldsymbol{u}$, $\boldsymbol{v}$ represent the left and right singular vectors, and σ are the corresponding singular values (with $\sigma_{i+1} \ge \sigma_i$). The essential idea is to consider the following orthogonal vector spaces, the "signal" space spanned by the top L_o right singular vectors of the system matrix A_p, and the "noise" space that is spanned by the remaining $N - L_o$ vectors. In the absence of noise, L_o would simply be the number of independent rows of the matrix A_p, and the signal and noise subspaces would be identical to the row and null spaces of the matrix A_p, respectively. However, in the presence of noise, the lower singular values amplify the noise from the measurements and lead to a large error in the solution. Thus, the solution sought is expanded as $\boldsymbol{x} = \boldsymbol{x}_s + \boldsymbol{x}_n$, corresponding to the signal and noise spaces, respectively, which are estimated as follows:

(i) Signal space estimation: this component, $\boldsymbol{x}_s$, is determined by a L_o-term truncation of the SVD of A_p as follows:

$$\boldsymbol{x}_s = \sum_{i=1}^{L_o} \left(\frac{\boldsymbol{u}_i^H \boldsymbol{b}}{\sigma_i} \right) \boldsymbol{v}_i.$$

An immediate question concerns the selection of the parameter L_o. This number is chosen using the Morozov discrepancy principle [19], where L_o is chosen as the smallest number such that $\|A_p \boldsymbol{x}_s - \boldsymbol{b}\|_2 < \epsilon$, where ϵ is the square root of the noise variance, which in many situations, is reasonably known. The problem is not very sensitive to the exact choice of L_o, as the remaining components are determined in the next stage; various studies have also corroborated this observation [15,16].

(ii) Noise space estimation: this component, $\boldsymbol{x}_n$, is determined from a priori information about the problem, based on the following observation: when the discrete Fourier transform (DFT) coefficients of the *true* tangential fields are computed (using a forward solver; see plots in Fig. 2), we observe that most of the coefficients are very low in magnitude, i.e., the solution exhibits sparsity in the DFT basis. This property can be exploited to reconstruct the EM fields by using ideas from compressive sensing [20], which penalizes the l_1 norm of the solution vector to promote sparse solutions. As per the rigorous requirements of compressive sensing, a sparse signal can be reconstructed from undersampled linear measurements provided that the sensing matrix follows the restrictive isometry property (RIP). Since the RIP is difficult to verify in practice, we heuristically apply compressive sensing ideas to our problem, a strategy that has gained popularity in the EM community [11] in recent times. Thus, holding $\boldsymbol{x}_s$ constant, the noise space estimation proceeds as per the following optimization problem:

$$\begin{aligned} &\underset{\boldsymbol{x}_n}{\text{minimize}}\ \|\mathcal{M}(\boldsymbol{x}_s + \boldsymbol{x}_n)\|_1 \\ &\text{subject to } \|A_p \boldsymbol{x}_n - (\boldsymbol{b} - A_p \boldsymbol{x}_s)\|_2 \le \epsilon, \\ &\|A_s \boldsymbol{x}_n - (\boldsymbol{b}_s - A_s \boldsymbol{x}_s)\|_2 \le \eta \end{aligned} \tag{10}$$

where $\mathcal{M} = \mathcal{F}$, $\mathcal{W}$, or $\mathcal{D}$ are the DFT, wavelet, or discrete cosine transform (DCT) bases, respectively, chosen as candidates for sparse representations.

4. NUMERICAL RESULTS

In this section, we present the numerical results for the prediction of spatial EM fields from measurements using the formulations described previously. We describe the simulation setup, define the error metrics, and then present the results for a varying number of objects. All simulations are programmed in MATLAB 2018b and executed on an Intel Core i7-7700 CPU running at 3.60 GHz, using 16 GB RAM.

A. Simulation Setup

The simulation domain is $10\lambda \times 10\lambda$ with four objects all with different permittivities and an outer wall which encloses all the objects. The simulation setup is shown in Fig. 3 with objects 1, 2, 3, and 4 centered at $(-2.5\lambda, 1.5\lambda)$, $(2\lambda, 2\lambda)$, $(1\lambda, -2.5\lambda)$, and $(-2.5\lambda, -1\lambda)$, respectively, where λ is the wavelength. The relative permittivities of the objects 1, 2, 3, 4, and wall are $\epsilon_{r1} = 3.7 - 2.1j$, $\epsilon_{r2} = 1.7 - 1.1j$, $\epsilon_{r3} = 2.7 - 3.7j$, $\epsilon_{r4} = 1.2 - 1.1j$, and $\epsilon_{rw} = 3.7 - 2.1j$, respectively (lossy, so as to mimic real-life materials such as a concrete wall, etc.). Object 1 is a square of side λ, object 2 is a circle with radius 0.75λ, object 3 is a rectangle with sides $1\lambda \times 2.5\lambda$, and object 4 is a circle with radius 1λ. Note that the permittivity and the true geometry of the objects are used only in the forward solver to generate the synthetic measurements. The source is placed at the location $\vec{r}_0 = (0.5\lambda, -0.75\lambda)$, with a cylindrical plane wave of the form: $\phi_{\text{inc}}(\vec{r}) = H_0^{(2)}(k_0|\vec{r} - \vec{r}_0|)$.

We obtain the true fields first using the boundary integral (BI) method using pulse basis for the tangential fields on the surface of the scatterers. Substituting the true tangential fields in Huygens' principle [Eq. (1)], fields at all other locations are obtained. For this problem, a spatial discretization of $\lambda/40$ is considered to ensure numerical convergence. To verify the correctness of our forward solver, we have simulated the scattering from a single infinite cylinder of radius λ and validated it with the Mie series solution, finding agreement within a relative error of 1.5%. Since the electric field integral equation is known to display numerical issues related to cavity resonances, we verify (numerically) that there are no resonances in the frequency range $f_0 \pm \frac{f_0}{3}$, where f_0 is the operating frequency in our simulations. The measurements are corrupted with additive white Gaussian noise (AWGN) with a signal to noise ratio (SNR) of 25 dB and 10 dB.

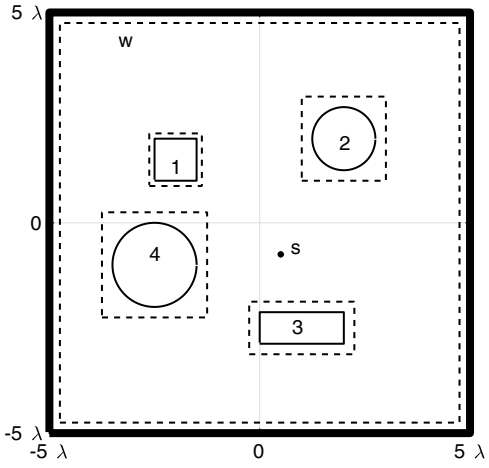

Fig. 3. Schematic of $10\lambda \times 10\lambda$ simulation domain. The domain includes a wall, four objects, and a source. The objects 1, 2, 3, and 4 have their centers respectively at $(-2.5\lambda, 1.5\lambda)$, $(2\lambda, 2\lambda)$, $(1\lambda, -2.5\lambda)$, and $(-2.5\lambda, -1\lambda)$. The source is located at $(0.5\lambda, -0.75\lambda)$ and "w" is the outer boundary. The dotted contours are the approximate geometry of the objects used in the field reconstruction algorithm.

B. Error Metric Definition

We define two error metrics in order to evaluate the performance of our method, namely the tangential field error, (Δ_T), and the error in reconstruction on the 2D grid, (Δ_G). The tangential field error is defined as follows:

$$\Delta_T = \frac{\|\boldsymbol{x}_{\text{est}} - \boldsymbol{x}_{\text{true}}\|_2}{\|\boldsymbol{x}_{\text{true}}\|_2}, \tag{11}$$

where $\boldsymbol{x}_{\text{est}}$ and $\boldsymbol{x}_{\text{true}}$ are the estimated and true tangential fields, respectively.

For the purpose of quantifying the accuracy of the predicted field, the field is estimated over the $10\lambda \times 10\lambda$ region that is discretized on a grid with pitch equal to $\lambda/20$.

The error in reconstruction is calculated using the following relation:

$$\text{error}(\Delta_G) = \frac{\|\boldsymbol{\phi}_{\text{est}} - \boldsymbol{\phi}_{\text{true}}\|_2}{\|\boldsymbol{\phi}_{\text{true}}\|_2}, \tag{12}$$

where $\boldsymbol{\phi}_{\text{est}}$ and $\boldsymbol{\phi}_{\text{true}}$ are the estimated and true fields over the 2D grid of points, respectively.

We also define the relative error at a location $\vec{r}$ as follows:

$$\frac{|\phi_{\text{est}}(\vec{r}) - \phi_{\text{true}}(\vec{r})|}{|\phi_{\text{true}}(\vec{r})|}, \tag{13}$$

where $\phi_{\text{est}}(\vec{r})$ and $\phi_{\text{true}}(\vec{r})$ are the estimated and true fields at $\vec{r}$, respectively.

The fields inside the object and fields that are very close to the scatterer surfaces (at a distance less than $\lambda/10$ from the approximate surfaces of the objects) are not considered in the error calculation.

C. Problem Discretizations

For predicting the field, we don't assume the knowledge of the exact shape of the scatterer, instead we approximate the geometry of the object by a bounding box that encloses the object. This is shown in Fig. 3 by means of dotted contours around the objects. The system matrix and the state matrix for the inverse problem [of the form given in Eq. (9)] are obtained using a uniform discretization of $\lambda/5$ along the dotted contours. This was chosen heuristically based on numerical experiments where the discretization was varied from $\lambda/2$ to $\lambda/20$; it was found that a discretization of $\lambda/5$ gives the optimal trade-off between accuracy and computational cost. The number of unknowns for

the tangential fields varies with the number of objects; considering all four objects and the wall, there are 704 unknowns. In the figures shown below, we consider the case of all 4 objects and the wall with 387 randomly chosen field measurements (0.55 times the number of unknowns) with 25 dB SNR. The system matrix A_p has a rank of 380, and using the Morozov principle gives a number, L_o, in the range of 140–150 as the number of significant singular values at this value of SNR (i.e., the signal space is spanned by the first L_o right singular vectors of A_p).

D. Applicability of Compressive Sensing When $M > \frac{N}{2}$

In the cases where the number of measurements M is greater than $\frac{N}{2}$, a natural question arises regarding whether or not there are more equations than the number of variables, and subsequently the applicability of the idea of compressive sensing. However, when we construct a "composite" system matrix such that $\tilde{A} = \begin{pmatrix} A_p \\ A_s \end{pmatrix}$ for various values of M and study its singular value spectrum, the following observations emerge:

(i) Even by the conservative definition of rank, which includes very small but non-zero singular values, the rank of the composite system does not exceed N.
(ii) If we take a more realistic scenario and consider singular values within a factor of 10^6 of the maximum singular value, the number of significant singular values is well below N.

Therefore, even though the composite matrix $\tilde{A}$ is overdetermined, it does not have full column rank. Thus, the use of a priori information toward compressive sensing solutions remains legitimate.

E. Predictions Based on Random Measurements

The reconstructed tangential fields on the wall are plotted along with the true tangential fields in Fig. 4. It can be seen that the tangential fields are recovered well.

To visualize field prediction, we consider a contour of radius 4.2λ centered at origin, which includes all objects, plot the true and predicted fields over it using the CS-SOM method, and report the results in Fig. 5. As can be seen, the prediction matches the true field very well. Next, to consider a larger area

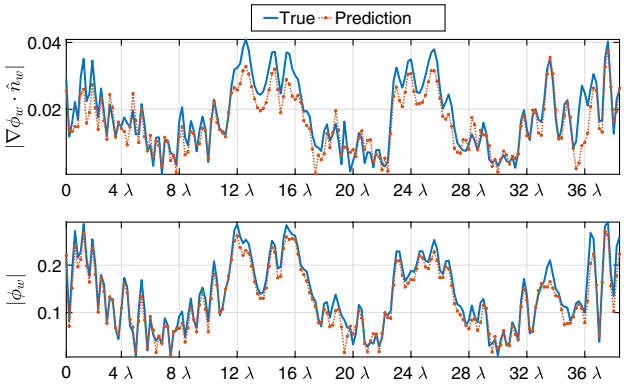

Fig. 4. Comparison of the magnitudes of the estimated and true tangential fields on the surface of the inexact wall, obtained for 387 measurements (0.55 times the number of unknowns). The measurements are noise corrupted by 25 dB SNR.

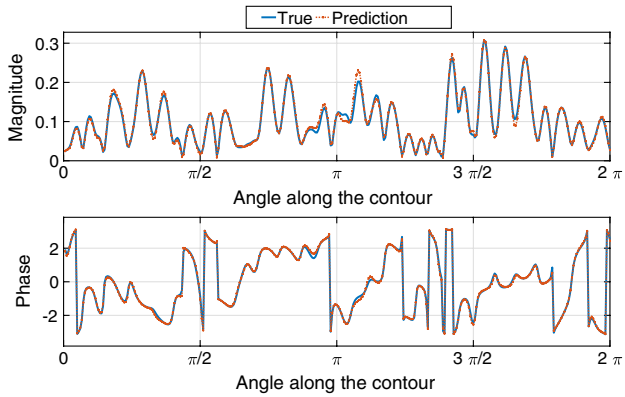

Fig. 5. Comparison of reconstructed and true fields (magnitudes and phase) over a contour of radius 4.2λ obtained for 0.55x sampling rate (387 measurements). The measurements are noise corrupted by 25 dB SNR.

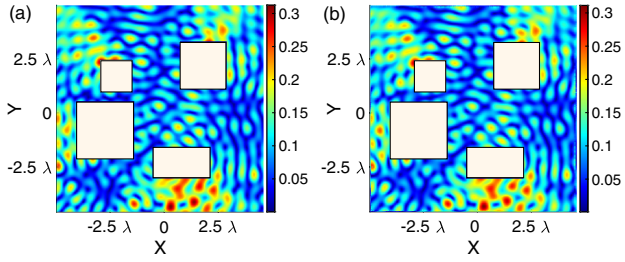

Fig. 6. Magnitude of (a) true and (b) reconstructed 2D fields over a 10λ × 10λ grid, obtained for 0.55x sampling rate (387 measurements). The measurements are noise corrupted by 25 dB SNR. The color bar shows the field magnitude in V/m.

for prediction, we consider the entire scattering region outside the objects, plotting the true and reconstructed fields in Figs. 6 and 7, which again reveal a very good correspondence. Finally, Table 1 shows the tangential field error and the error in reconstruction for various measurement modalities (different numbers of measurements and SNR values). We also report along with the number of measurements, the *sampling rate* (SR) which is defined as the ratio of the number of measurements to the number of unknowns in the problem. We use the DCT bases and apply the subspace optimization method [see Eq. (10)] for estimating the tangential fields.

In order to study how well our results generalize to different scattering geometries, we also perform experiments with different numbers of objects (two to four). Table 2 shows the tangential field error and the error in reconstruction with different numbers of objects with a fixed SR of 0.55. As can be seen, the predictions are quite accurate, giving an error of 12% for an SR of 0.55 and 25 dB SNR with a simulation time of 5 min per instance of random measurement points. The relative error at each location is shown in Fig. 8, and it can be seen that though the error observed is 12% for a 0.55x SR, the major error occurs near the boundary of the walls and in between close objects. As evidenced by the histogram of error values reported in Fig. 8(b), the prediction accuracy is very good at all the other regions and is less than 10% for more than 80% of the grid locations.

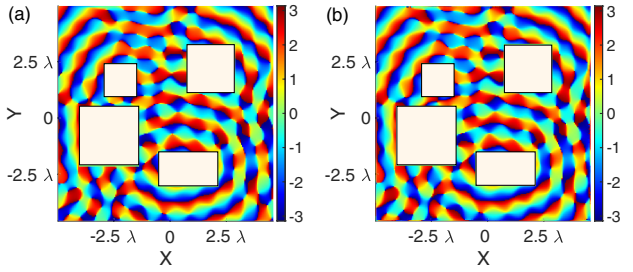

Fig. 7. Phase of (a) true and (b) reconstructed 2D fields over a 10λ × 10λ grid, obtained for 0.55x sampling rate (387 measurements). The measurements are noise corrupted by 25 dB SNR. The color bar shows the phase in radians.

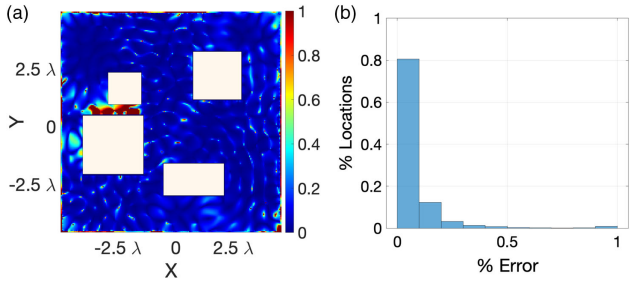

Fig. 8. (a) Relative error [see Eq. (13)] in the prediction of total field over a 10λ × 10λ grid discretized at λ/20. The prediction is obtained for 0.55x sampling rate (387 measurements). The measurements are noise corrupted by 25 dB SNR, and (b) histogram of normalized error over different locations of the simulation domain in (a). 80% of the locations have less than 10% prediction error with an average error of 12%.

Table 1. Percentage Error in the Predicted Field (Δ_G) and Recovered Tangential Field (Δ_T) for Different Measurement Modalities (Different Numbers of Measurements and SNR Values) over a 10λ × 10λ Grid Calculated for 100 Monte Carlo Trials[a]

		Measurements/Sampling Rate					
		212/ 0.3x		387/0.55x		563/0.8x	
SNR (dB)		Δ_G	Δ_T	Δ_G	Δ_T	Δ_G	Δ_T
25	Mean	23	32	12	22	8	19
	Max	32	43	17	29	11	24
	Min	15	24	7	17	5	16
	SD	3	3	2	3	1	2
10	Mean	45	45	31	36	24	30
	Max	54	53	37	41	28	39
	Min	39	39	25	30	20	24
	SD	3	3	2	3	2	3

[a]Abbreviation: SD, standard deviation.

Table 2. Percentage Error in the Predicted Field (Δ_G) and Recovered Tangential Field (Δ_T) for Different Numbers of Objects over a 10λ × 10λ Grid, for 0.55x Sampling Rate[a]

		Number of Objects					
		2		3		4	
SNR (dB)		Δ_G	Δ_T	Δ_G	Δ_T	Δ_G	Δ_T
25	Mean	10	17	9	17	12	22
	Max	19	13	14	22	17	29
	Min	6	25	6	14	7	11
	SD	3	3	2	2	2	3
10	Mean	30	31	30	32	31	36
	Max	37	38	39	46	37	47
	Min	24	25	27	28	25	30
	SD	3	3	2	4	2	3

[a]The error was calculated for 100 Monte Carlo trials. The numbers of objects are considered in serial wise as shown in Fig. 3. Abbreviation: SD, standard deviation.

F. Note on Related Numerical Schemes

It is worth mentioning in passing, the accuracy of three related schemes in solving the previously mentioned problem.

(i) It is natural to consider a truncated SVD (of the composite matrix $\tilde{A}$) when faced with finding the solution to a linear inverse problem with noisy data. Since this approach does not leverage any a priori information about the problem, the error, not surprisingly, is higher. In particular, we obtain $\Delta_G = 19\%$ and $\Delta_T = 30\%$ in the case of an SR of 0.55 and 25 dB SNR when we retain the minimum number of singular terms so as to satisfy $\|A_p \boldsymbol{x} - \boldsymbol{b}\|_2 < \epsilon$.

(ii) The second approach is to use compressive sensing in a straight forward manner by formulating the problem as follows:

$$\begin{aligned} &\underset{\boldsymbol{\xi}}{\text{minimize}} \ \|\boldsymbol{\xi}\|_1 \\ &\text{subject to } \|A_p K\boldsymbol{\xi} - \boldsymbol{b}\|_2 \le \epsilon\,, \\ &\|A_s K\boldsymbol{\xi} - \boldsymbol{b}_s\|_2 \le \eta \end{aligned} \tag{14}$$

where sparsity of the solution in a domain represented by a linear transformation K with coefficients $\boldsymbol{\xi}$ is leveraged for obtaining a solution. Since exact knowledge of the sparsifying domain is not known in general, this approach also leads to a higher error. In our experiments, we considered the DFT, DCT, and Wavelet (db-2) transformations, achieving an average of $\Delta_G = 14\%$ and $\Delta_T = 25\%$ in the case of an SR of 0.55 and 25 dB SNR. Our proposed CS-SOM approach gives superior results and can be thought of as a synthesis of these two "naive" approaches.

(iii) The third approach is to enforce sparsity by choosing the lower frequency DFT coefficients as the unknowns. We compare CS-SOM to two such reconstruction algorithms, namely the New FFT (NFFT) SOM [21] and the FFT—Twofold SOM (T-SOM) [22]. We find that for an SR of 0.55 and 25 dB SNR, both NFFT SOM and T-SOM achieve an average of $\Delta_G = 15\%$ and $\Delta_T = 30\%$. We do note, however, that CS-SOM has a higher computational run time than NFFT SOM or T-SOM.

5. DISCUSSION

A. Sparsity in Electromagnetic Reconstruction Problems

In this paper, we have proposed a method of field reconstruction using EM principles (Huygens' principle, Extinction theorem) and tangential field sparsity in certain transformed domains. A natural question arises regarding the applicability of sparse reconstruction in general EM problems. This issue has been addressed in [22] (Fig. 6.14). As it turns out, the right singular vectors corresponding to the highest singular values of the state operator resemble low-frequency Fourier bases, whereas those corresponding to the lower singular values resemble high-frequency Fourier bases. If we consider the simple idea of the pseudoinverse of the operator, it becomes clear that the solution is dominated by the highest singular values and, therefore, the low-frequency bases. Hence, the idea of imposing sparsity is a general principle in all EM problems involving radiation-like operators.

B. Extensions of This Work

An interesting line of research opens up when we consider the optimality of the sampling locations. To understand this point better, we conducted numerical experiments in which we made field measurements only along an arbitrary line, and found the field prediction to be erroneous. Motivated by this observation, we plan to extend our work by investigating optimal sensor placement and optimal sensing basis with an aim to minimize the number of measurements. There has been promising recent work, both theoretical and computational, in this regard [23–28], though in different settings than those considered here.

Currently, we characterize the error using the SR which is defined as the ratio between the number of measurements and the number of unknowns. The latter is not a fundamental choice and other characterizations, such as the electrical length of the scatterers or the degrees of freedom of the scattered fields [29,30], are also possible.

An important line of research is to consider the case of phaseless (amplitude-only) measurements. Such an extension would be useful in situations where it is inconvenient/expensive to make measurements with phase. This problem is called "Phase Retrieval" and has been studied extensively in the literature [31–34]. Traditional approaches like alternating projections [35,36] often reach a local minima, but more recent advances in this area are based on dictionary learning [37,38] and have achieved considerable success, even for the case where the number of measurements is smaller than the number of unknowns. Finally, we plan to extend our work to three-dimensional (3D) scenarios.

C. Limitations of the Proposed Method

The method proposed in this paper suffers from the following limitations:

(i) The highest error in prediction occurs at the corners of the outer wall and the regions in between the objects where very few field measurements are taken. To mitigate the error in between the objects, more measurements should be considered in such regions.

(ii) In complex scattering environments with a large number of scatterers, the number of unknowns increases. Since the error in reconstruction depends on the SR, the number of measurements needed to attain the same level of accuracy is also higher. Further studies on the degrees of freedom inherent in a scattering environment need to be undertaken in order to determine how the number of unknowns scale with the number of scatterers [29,30,39].

D. Summary

In this work, we have shown that when spatial measurements of fields are taken in an indoor scenario, we can recover the EM fields to varying degrees of accuracy depending on the number and location of measurements. We use the compressive sensing subspace optimization technique to find tangential fields on the surfaces of the scatterers. For example, in the numerical study, we undertook within a $10\lambda \times 10\lambda$ region, the EM fields can be recovered with 387 measurements up to an error of $\approx$12%.

E. Future Applications

The method described in this paper can be employed in a number of scenarios, a few of which are mentioned here. Since our method correctly reconstructs the tangential fields on a contour bounding the object, a logical extension is the prediction of the radar cross-section (RCS) of the scattering object using a near-to-far field transformation (e.g., see [1]). RCS estimation is known to be a time-intensive process, and any improvement that can be attained by minimizing the number of measurements required is welcome. Next, indoor positioning systems can employ this method, instead of ray tracing methods (e.g., [40–42]) to determine the location of a person based on EM field measurements. To counter uniqueness problems (where two or more locations have approximately the same field magnitude), multiple frequency sources can be employed, and/or data can be collected from several locations. Finally, our method can also be applied to Wi-Fi access point planning, in which one tries to optimally place Wi-Fi routers in an environment so that most locations receive good quality of service (QoS) guarantees.

Acknowledgment. We are very grateful to the anonymous reviewers for providing valuable feedback that has led to a significant improvement in the quality of our manuscript.

Disclosures. The authors declare no conflicts of interest.

[†]These authors contributed equally to this work.

REFERENCES

1. T. B. Hansen, R. A. Marr, U. H. Lammers, T. J. Tanigawa, and R. V. McGahan, "Bistatic rcs calculations from cylindrical near-field measurements–part i: theory," IEEE Trans. Antennas Propag. **54**, 3846–3856 (2006).
2. L. Pei, R. Chen, J. Liu, H. Kuusniemi, T. Tenhunen, and Y. Chen, "Using inquiry-based bluetooth rssi probability distributions for indoor positioning," J. Glob. Position. Syst. **9**, 122–130 (2010).

3. Z.-H. Wu, Y. Han, Y. Chen, and K. R. Liu, "A time-reversal paradigm for indoor positioning system," IEEE Trans. Veh. Technol. **64**, 1331–1339 (2015).
4. A. Bose and C. H. Foh, "A practical path loss model for indoor wifi positioning enhancement," in *Information, Communications & Signal Processing, 2007 6th International Conference on* (IEEE, 2007), pp. 1–5.
5. A. Toscano, F. Bilotti, and L. Vegni, "Fast ray-tracing technique for electromagnetic field prediction in mobile communications," IEEE Trans. Mag. **39**, 1238–1241 (2003).
6. V. Degli-Esposti, D. Guiducci, A. de'Marsi, P. Azzi, and F. Fuschini, "An advanced field prediction model including diffuse scattering," IEEE Trans. Antennas Propag. **52**, 1717–1728 (2004).
7. Z. Ji, B.-H. Li, H.-X. Wang, H.-Y. Chen, and T. K. Sarkar, "Efficient ray-tracing methods for propagation prediction for indoor wireless communications," IEEE Antennas Propag. Mag. **43**, 41–49 (2001).
8. K. A. Remley, H. R. Anderson, and A. Weisshar, "Improving the accuracy of ray-tracing techniques for indoor propagation modeling," IEEE Trans. Veh. Technol. **49**, 2350–2358 (2000).
9. W. C. Chew, *Waves and Fields in Inhomogeneous Media* (IEEE, 1995).
10. S. Boyd and L. Vandenberghe, *Convex Optimization* (Cambridge University, 2004).
11. A. Massa, P. Rocca, and G. Oliveri, "Compressive sensing in electromagnetics-a review," IEEE Antennas Propag. Mag. **57**, 224–238 (2015).
12. G. Oliveri, M. Salucci, N. Anselmi, and A. Massa, "Compressive sensing as applied to inverse problems for imaging: Theory, applications, current trends, and open challenges," IEEE Antennas Propag. Mag. **59**, 34–46 (2017).
13. F. Viani, L. Poli, G. Oliveri, F. Robol, and A. Massa, "Sparse scatterers imaging through approximated multitask compressive sensing strategies," Microw. Opt. Technol. Lett. **55**, 1553–1558 (2013).
14. M. Bevacqua, L. Crocco, L. Di Donato, and T. Isernia, "Microwave imaging of nonweak targets via compressive sensing and virtual experiments," IEEE Antennas Wireless Propag. Lett. **14**, 1035–1038 (2014).
15. X. Chen, "Subspace-based optimization method for solving inverse-scattering problems," IEEE Trans. Geosci. Remote Sens. **48**, 42–49 (2009).
16. Y. Sanghvi, Y. N. G. B. Kalepu, and U. Khankhoje, "Embedding deep learning in inverse scattering problems," IEEE Trans. Comput. Imaging **6**, 46–56 (2019).
17. C. A. Balanis, *Advanced Engineering Electromagnetics* (Wiley, 1999).
18. D. K. Sastry, C. Bhat, and U. K. Khankhoje, "Spatial prediction of undersampled electromagnetic fields," in *PhotonIcs & Electromagnetics Research Symposium-Spring (PIERS-Spring)* (IEEE, 2019), pp. 131–138.
19. V. Morozov and A. Grebennikov, *Methods for Solution of Ill-Posed Problems: Algorithmic Aspects* (Moscow University, 2005).
20. E. J. Candès and M. B. Wakin, "An introduction to compressive sampling [a sensing/sampling paradigm that goes against the common knowledge in data acquisition]," IEEE Signal Process. Mag. **25**, 21–30 (2008).
21. Z. Wei, R. Chen, H. Zhao, and X. Chen, "Two FFT subspace-based optimization methods for electrical impedance tomography," Progr. Electromag. Res. **157**, 111–120 (2016).
22. X. Chen, *Computational Methods for Electromagnetic Inverse Scattering* (Wiley, 2018).
23. S. Joshi and S. Boyd, "Sensor selection via convex optimization," IEEE Trans. Signal Process. **57**, 451–462 (2008).
24. J. Ranieri, A. Chebira, and M. Vetterli, "Near-optimal sensor placement for linear inverse problems," IEEE Trans. Signal Process. **62**, 1135–1146 (2014).
25. C. Jiang, Y. C. Soh, and H. Li, "Sensor placement by maximal projection on minimum eigenspace for linear inverse problems," IEEE Trans. Signal Process. **64**, 5595–5610 (2016).
26. S. Liu, S. P. Chepuri, M. Fardad, E. Maşazade, G. Leus, and P. K. Varshney, "Sensor selection for estimation with correlated measurement noise," IEEE Trans. Signal Process. **64**, 3509–3522 (2016).
27. R. Obermeier and J. A. Martinez-Lorenzo, "Sensing matrix design via mutual coherence minimization for electromagnetic compressive imaging applications," IEEE Trans. Comput. Imaging **3**, 217–229 (2017).
28. R. Solimene, M. A. Maisto, and R. Pierri, "Sampling approach for singular system computation of a radiation operator," J. Opt. Soc. Am. A **36**, 353–361 (2019).
29. O. M. Bucci and G. Franceschetti, "On the degrees of freedom of scattered fields," IEEE Trans. Antennas Propag. **37**, 918–926 (1989).
30. R. Piestun and D. A. Miller, "Electromagnetic degrees of freedom of an optical system," J. Opt. Soc. Am. A **17**, 892–902 (2000).
31. P. Netrapalli, P. Jain, and S. Sanghavi, "Phase retrieval using alternating minimization," in *Advances in Neural Information Processing Systems 26*, C. J. C. Burges, L. Bottou, M. Welling, Z. Ghahramani, and K. Q. Weinberger, eds. (Curran Associates, Inc., 2013), pp. 2796–2804.
32. E. J. Candes, Y. C. Eldar, T. Strohmer, and V. Voroninski, "Phase retrieval via matrix completion," SIAM Rev. **57**, 225–251 (2015).
33. K. Jaganathan, Y. C. Eldar, and B. Hassibi, "Phase retrieval: an overview of recent developments," in *Optical Compressive Imaging*, A. Stern, ed. (Taylor & Francis Group, 2015).
34. J. Sun, Q. Qu, and J. Wright, "A geometric analysis of phase retrieval," Found. Comput. Math. **18**, 1131–1198 (2018).
35. R. Gerchberg and W. Saxton, "A practical algorithm for the determination of the phase from image and diffraction plane pictures," Optik **35**, 237–246 (1972).
36. J. R. Fienup, "Phase retrieval algorithms: a comparison," Appl. Opt. **21**, 2758–2769 (1982).
37. A. M. Tillmann, Y. C. Eldar, and J. Mairal, "Dolphin–dictionary learning for phase retrieval," IEEE Trans. Signal Process. **64**, 6485–6500 (2016).
38. T. Qiu and D. P. Palomar, "Undersampled sparse phase retrieval via majorization–minimization," IEEE Trans. Signal Process. **65**, 5957–5969 (2017).
39. J. Xu and R. Janaswamy, "Electromagnetic degrees of freedom in 2-d scattering environments," IEEE Trans. Antennas Propag. **54**, 3882–3894 (2006).
40. A. Tayebi, J. Gomez Perez, F. M. S. D. Adana Herrero, and O. Gutierrez Blanco, "The application of ray-tracing to mobile localization using the direction of arrival and received signal strength in multipath indoor environments," Progr. Electromag. Res. **91**, 1–15 (2009).
41. C. Sturm, W. Sorgel, T. Kayser, and W. Wiesbeck, "Deterministic uwb wave propagation modeling for localization applications based on 3d ray tracing," in *IEEE MTT-S International Microwave Symposium Digest* (IEEE, 2006), pp. 2003–2006.
42. O. Katircioglu, H. Isel, O. Ceylan, F. Taraktas, and H. B. Yagci, "Comparing ray tracing, free space path loss and logarithmic distance path loss models in success of indoor localization with rssi," in *19th Telecommunications Forum (TELFOR) Proceedings of Papers* (IEEE, 2011), pp. 313–316.